forum acusticum 2023

# ACTIVE REALISATION OF THE INERTER BY RELATIVE ACCELERATION FEEDBACK

**Srećko Arandia-Krešić**[1*] **Neven Alujević**[1] **Stipe Turalija**[1]
**Marin Jalšić**[2]

[1] Faculty of Mechanical Engineering and Naval Architecture, University of Zagreb, Croatia
[2] AVL-AST d.o.o, Zagreb, Croatia

## ABSTRACT

Physical realisations of the inerter are either large-scale, i.e., rack and pinion inerters, or they inherently include additional elements in parallel or in series with the inerter, i.e., shunted electromechanical transducers or active force feedback inerter realisations, or alternatively, they bring along large parasitic damping, i.e., fluid-based inerters. This study investigates whether a small-scale inerter may be realised by feeding back subtracted outputs of two accelerometers attached to the two mechanical terminals of an electrodynamic force actuator. Although in theory such a feedback loop is unconditionally stable due to the collocated transducer arrangement, in practice, the feedback loop is shown to be only conditionally stable. This is due to the lack of duality between the sensors and the actuator in conjunction with the intrinsic dynamics of the transducers. Therefore, a fully coupled model including the dynamics of the two inertial accelerometers and the electrodynamic actuator is developed. This model is then coupled to a two-degree-of-freedom mechanical oscillator to study the feedback loop's stability and maximum achievable inertance. It is shown experimentally that the inertance can be realised which is about five times the mass of the actuator before the system becomes unstable.

[*] ***Srećko Arandia-Krešić***: *sarandia@fsb.hr*



**Keywords:** inerter, active vibration control, vibration isolation

## 1. INTRODUCTION

Inerter is a one-port, two-terminal element in mechanical networks which resists relative acceleration across its two terminals. The coefficient of this resistance, the inertance, is measured in kilograms. The inerter fills an empty niche enabling a complete analogy between mechanical and electrical networks, where, assuming the force-current analogy, the electrical analogue of the inerter is the capacitor [1,2]. In the framework of mechanical network analysis, it is typically assumed that the inerter behaves in an idealised way, i.e., that it can be represented through its inertance only. Such idealisations are ordinarily assumed for elements like springs, dampers, inductances or resistors in lumped parameter mechanical or electrical networks. However, a realistic element, for example a helical spring, can itself exhibit a rich dynamic behaviour [3]. This is equally true for other elements of lumped parameter mechanical systems including the inerter as discussed in the following paragraph.

Typical mechanical inerter designs include rack and pinion inerters [4], ball-screw inerters [5], and helical fluid channel inerters [6]. One of the most important characteristics of any physical realisation of the inerter is the ratio of its inertance to its mass. This ratio is normally required to be large to enhance inertia effects of lightweight structures without significantly increasing their mass. In mechanical inerter designs the inertance can be several hundred

times larger than the mass of the inerter itself [4]. However, such inerters are typically mid- to large-scale and are not suitable for vibration control purposes in small scale applications due to their large dimensions and large stroke. Furthermore, effects such as friction, stick-slip of the gear pairs, or the elasticity of the gears and connecting rods are inevitably present in gear-train inerter constructions. On the other hand, a relatively large parasitic non-linear damping characterises the fluid-based inerters [6].

Another class of inerter realisations are the electromechanical inerters. In these systems electomechanical transducers are shunted with appropriate electrical impedances at their electrical ports in order to generate inertance-like effects at their mechanical ports. Small scale electromechanical transducers are characterised by a relatively low energy conversion efficiency [7], so it is necessary to use non-Foster shunt circuits in order to compensate for losses in the transducers [8]. This makes the approach active, which on one hand requires energy and on the other a careful regard of the stability and robustness of the system. Nevertheless, it is possible to realise an ideal inerter element connected to additional elements that occur as a side-effect of using a particular shunting technique. For example, by shunting a voice coil transducer with a certain negative impedance electrical circuit, inerter connected in series with a parallel spring damper-pair can be realised [8]. The additional lumped parameter elements in the equivalent mechanical network may or may not be desirable.

Further active approaches to realise the inerter include the force feedback approach [9,10]. Here a pair of collocated reactive actuators and a force sensor are used to feed back the output of the force sensor through both single and double integrators to drive the actuator. In such a way the inerter can be realised which is connected in series with a damper [10].

In this paper, an attempt is made to realise the inerter by direct acceleration feedback control system. Outputs of two accelerometers mounted at the two terminals of a force actuator are subtracted to form a relative acceleration error signal which is amplified through an adjustable gain and fed to the actuator. In this way it may be possible to realise a small-scale inerter with an actively tuneable inertance without additional elements in parallel or in series to the inerter. Classical inertial accelerometers and a small-scale voice-coil actuator are used.

A fully coupled electromechanical model of a two degree of freedom mechanical system equipped with the described active control loop is formulated in this paper. The dynamics of the inertial accelerometers and the electrodynamic actuator are modelled in detail. The coupled model is used to study the stability of the feedback loop and to assess the range of realisable inertances that could be used to isolate simple harmonic discrete vibrations coming from a flexible base to sensitive equipment mounted on it In the third section of the paper experimental analysis is given which was carried out using a dedicated 3D-printed test rig.

## 2. THEORETICAL CONSIDERATIONS

### 2.1 Mathematical model

The mechanical system considered is a lumped parameter two degree of freedom (DOF) system shown in **Figure 1**. This system is a representation of the vibration isolation problem in which the sensitive equipment, $m_2$, is suspended with a spring $k_2$ and a damper $c_2$ onto a flexible base characterized by the mas $m_1$, stiffness $k_1$ and a damper $c_1$. Dynamic excitation is applied to the base mass through the simple harmonic primary force $f_p$. The formulation presented considers time-harmonic functions, which are defined in complex form $f(t) = Re\{f(\omega)e^{i\omega t}\}$ , where $f(\omega)$ is the complex amplitude, $\omega$ is the circular frequency and $i = \sqrt{-1}$. As normally done in vibration studies, the formulation that follows thus refers to the complex amplitudes $f(\omega)$ of the time-harmonic functions $f(t)$ and, for brevity, the frequency dependence is omitted.

As discussed in, for example reference [11] with the inclusion of the inerter of inertance $b_2$ into the suspension, **Figure 1** (b), an antiresonance can be assigned to the transfer admittance between the primary force, $f_p$, and the displacement of the sensitive equipment, $m_2$, at the frequency $\omega_a = \sqrt{\frac{k_2}{b_2}}$, where subscript $a$ denotes the antiresonance. If the damping coefficient $c_2$ is made low, this creates a sharp dip in the transfer admittance amplitude and the corresponding 90-degree phase lead, so that the

mass $m_2$ becomes unresponsive to simple harmonic forcing at $\omega = \omega_a$. Therefore, a vibration isolation effect can be achieved provided that the inertance $b_2$ can be tuned to match the antiresonance frequency to the excitation frequency. If a small-scale mechanical system is considered, then existing inerter designs probably cannot accomplish the task for reasons discussed in Introduction. Therefore, it is reasonable to attempt to realise the inerter effects by using the feedback control loop shown schematically in **Figure 1** (a). The purpose of the feedback loop is to generate a control force proportional to the relative acceleration between the equipment and the base, that is, to emulate effects of the inerter, $b_2$, mounted in parallel to the suspension spring and damper, shown in **Figure 1**(b).

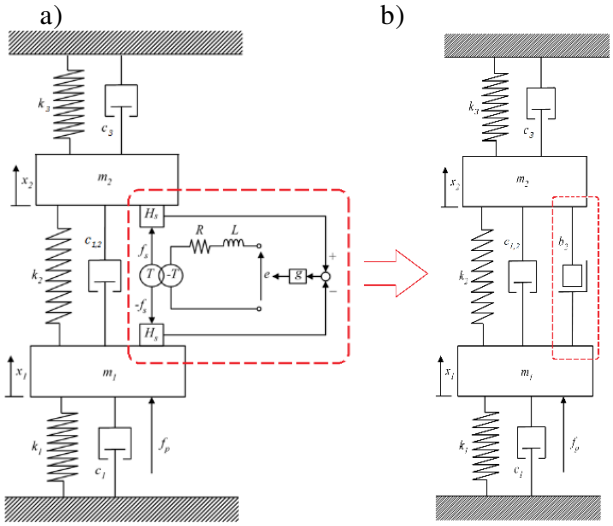


**Figure 1.** The 2 DOF mechanical system equipped with a direct acceleration feedback loop, plot (a), with the purpose of synthesizing the inerter, plot (b)

The control force, $f_c$, is applied by an electrodynamic actuator that reacts between the two masses. The actuator is characterized by a transducer coefficient *T,* which is often referred to as voice coil constant, inductance *L*, and the resistance *R*. The force generated by the actuator is proportional to the electrical current flowing through the transducer coil through the transducer coefficient *T*:

$$f_c = -Ti \tag{1}$$

The current *i,* however, depends both on the voltage applied at the transducer electrical terminals, *e*, and on the relative velocity, $s(x_2 - x_1)$, between its mechanical terminals, according to the following expression:

$$e = Ri + sLi + sT(x_2 - x_1) \tag{2}$$

where $s = i\omega$ is the Laplace variable.

In the present controller scheme the voltage, *e*, is made proportional to subtracted outputs of the two accelerometer sensors through a voltage amplifier gain, *g*, **Figure 1** (a). The error signals are provided by two equal inertial accelerometers characterised by the transfer function $H_s$. This is the frequency response function (FRF) between the accelerometer output and the true acceleration of a structure onto which the accelerometer is attached. The two accelerometers are assumed to be much lighter than the sensitive equipment or the flexible base, so that their mechanical impedance can be entirely neglected. Therefore, the voltage at the actuator electrical terminals is given by the control law:

$$e = gH_s s^2(x_2 - x_1) \tag{3}$$

The dynamics of the mechanical parts of the system, i.e. the system without the control loop elements encircled by the red dashed line in **Figure 1** can be represented by four mobility functions $Y_{i,j}$, *i,j=1..2*. They are the FRFs between the velocity of the mass *i* due to a force acting at the mass *j*. If *i=j* the corresponding mobility is referred to as driving point mobility, otherwise it is referred to as a transfer mobility. By considering contributions of the primary and the control forces one can write:

$$sx_1 = Y_{1,1}f_p - Y_{1,1}f_c + Y_{1,2}f_c \tag{4}$$

$$sx_2 = Y_{2,2}f_p - Y_{2,1}f_c + Y_{2,2}f_c \tag{5}$$

By considering Eqs. (1-5) and the reciprocity principle that imposes $Y_{2,1} = Y_{1,2}$, the fully coupled closed loop response of the system can be calculated in terms of five FRFs:

$$H_{e,f_p} = \frac{sgH_s(Y_{1,2} - Y_{1,1})(R + Ls)}{D_1}, \tag{6}$$

$$H_{i,f_p} = \frac{(Y_{1,1} - Y_{1,2})(T - sgH_s)}{D_1}, \tag{7}$$

$$H_{f_c,f_p} = -TH_{i,f_p}, \tag{8}$$

$$H_{x_1 f_p} = \frac{\left\{\begin{matrix}(Y_{1,2}^2 - Y_{1,1}Y_{2,2})T^2 + \\ +sgH_s(Y_{1,1}Y_{2,2} - Y_{1,2}^2)T + \\ +Y_{1,1}(R+Ls)\end{matrix}\right\}}{D_1 s}, \quad (9)$$

$$H_{x_2 f_p} = \frac{\left\{\begin{matrix}(Y_{1,2}^2 - Y_{1,1}Y_{2,2})T^2 + \\ +sH_s(Y_{1,1}Y_{2,2} - Y_{1,2}^2)T + \\ +Y_{1,2}(R+Ls)\end{matrix}\right\}}{D_1 s}, \quad (10)$$

where

$D_1 = (2Y_{1,2} - Y_{1,1} - Y_{2,2})T^2 + gH_s(Y_{1,1} - 2Y_{1,2} + Y_{2,2})sT + R + Ls$

, $H_{e,f_p}$ is the FRF between the actuator voltage and the primary excitation force, $H_{i,f_p}$ is the FRF between the actuator current and the primary excitation force, $H_{f_c,f_p}$ is the FRF between the control force and the primary excitation force, $H_{x_1,f_p}$ is the closed loop driving point receptance, and $H_{x_2,f_p}$ is a closed loop transfer receptance.

The sensor-actuator open loop FRF can be obtained by calculating the FRF between the subtracted accelerometer outputs and the voltage fed to the actuator in absence of the primary excitation:

$$H_{s,a} = s^2 H_s \left(x_2 - x_1\right)\Big|_{f_p=0}, \quad (1)$$

This can be done by substituting $f_p = 0$ into Eqs. (4,5) and considering also Eqs. (1-3):

$$H_{s,a} = \frac{sH_s T\left(2Y_{1,2} - Y_{2,2} - Y_{1,1}\right)}{\left(2Y_{1,2} - Y_{2,2} - Y_{1,1}\right)T^2 + R + Ls}, \quad (2)$$

The transfer function $H_s$ characterising the two accelerometer sensors can be written as [12]:

$$H_s = \frac{\omega_A^2}{\omega_A^2 + 2\zeta_A \omega_A s + s^2}, \quad (3)$$

where $\omega_A$ is the mounted natural frequency of the accelerometer, and $\zeta_A$ is the accelerometer damping ratio. For simplicity, it is assumed that the accelerometer sensitivity is absorbed in the feedback gain *g*. In other words, the accelerometer transfer function has been normalised to have a unit sensitivity for static accelerations.

The four mechanical mobility functions $Y_{i,j}$ have been calculated in, for example, reference [11].

### 2.2 Stability

Although the control approach is physically well-founded, its application is not straightforward. For example, the relative acceleration sensor is collocated to the reactive force actuator, but the two transducers are not dual [13,14], i.e., they are not complementary in terms of mechanical power. As a result, the inherent frequency response of the sensor-actuator transducers can inhibit the stability of the feedback loop, as discussed in reference [15]. In order to assess the stability of the feedback loop, Nyquist criterion is used. The sensor-actuator open-loop FRF, Eq. (2), is first analysed for an example small-scale vibration isolation problem. The properties of this model problem system are given in Table 1.

**Table 1:** Parameters of the system

| parameter | value |
|---|---|
| $m_1$ | 0,045 kg |
| $m_2$ | 0,06075 kg |
| $c_{1,2}$ | 0.8Ns/m |
| $k_1$ | 55400 N/m |
| $k_2$ | 9100 N/m |
| $k_3$ | 18150 N/m |
| $T$ (N/A,Vs/m) | 0.45 |
| $L$ ($\cdot 10^6$ H) | 63 |
| $R$ ($\Omega$) | 1.5 |

The properties of the actuator correspond to an off-the-shelf miniature moving coil linear motor [16]. The mounted natural frequency and the damping ratio of the two accelerometers are: $f_a = \frac{\omega_A}{2\pi} = 42$ kHz and $\zeta_A = 0.0158$.

**Figure 2** shows the Nyquist plot of the sensor-actuator open-loop FRF considering the transducer dynamics. Although the locus is predominantly in the positive imaginary two quadrants of the

complex plane, as one would expect from a collocated force-acceleration transducer system, it nevertheless crosses towards the negative imaginary quadrants with a crossover of the negative real axis. This crossover occurs near the natural frequency of the accelerometer transducers. Furthermore, due to the combined effects of the low-pass filter and the voltage command approach, the locus is slightly rotated in the clockwise direction.

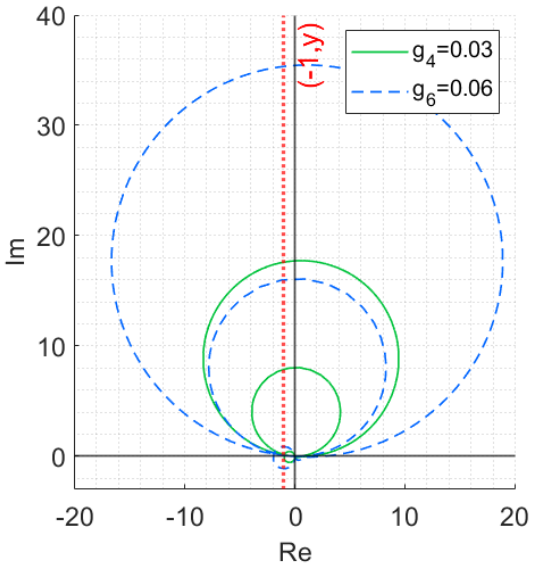


**Figure 2.** The Nyquist plot of the sensor-actuator open-loop frequency response function obtained theoretically.

This effect is beneficial for the stability of the feedback loop. This is because the contribution of the very high frequency sensor resonance (42 kHz) to the open-loop sensor-actuator FRF becomes attenuated, making the amplitude of the FRF at the crossover frequency much smaller than it would be with a current-command control. Note that the voltage command in effect results in a low-pass filter with a cut-off frequency of about 3.5 kHz. This cut-off frequency is the frequency of the pole of the *R-L* electrical subsystem with values like in Table 1. In conclusion, the system can be made stable (green solid line in **Figure 2**) if the feedback gain is below a certain value (about 0.03 Vs/m) but will go unstable if the feedback gain is increased above this threshold (blue dashed line).

When the active control is switched on, the transfer mobility between the primary force acting on mass $m_1$ and the velocity of mass $m_2$ becomes characterized by the antiresonance which can be tuned by increasing the feedback gain until instability occurs. **Figure 3** shows the transfer mobility of the active system with increasing feedback gains obtained theoretically.

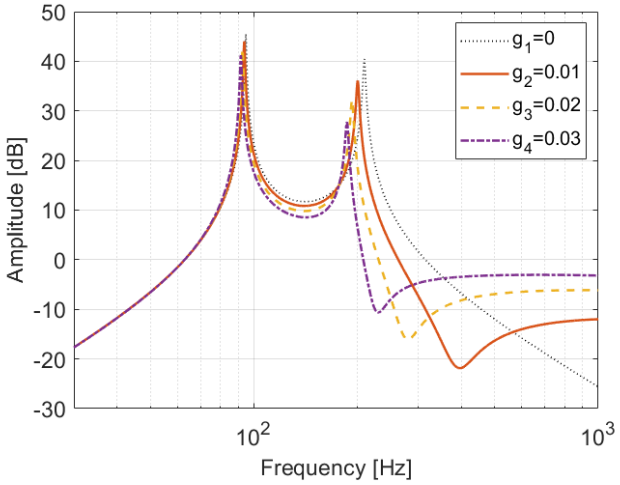


**Figure 3.** The transfer mobility of the active system with increasing feedback gains obtained theoretically.

As the feedback gain increases the antiresonance frequency shifts downwards with the lowest obtainable frequency of about 220 Hz due to the stability limit. This antiresonance frequency indicates the actively realised inertance of about 4.7 grams given that $\omega_a = \sqrt{\frac{k_2}{b_2}}$, see reference [11].

## 3. EXPERIMENTAL ANALYSIS

The experimental setup is shown in **Figure 4**. Note that the setup mimics the lumped parameter model in that the masses are manufactured by concentrating fairly rigid lumps of material whereas the stiffnesses are manufactured by lightweight flexible straight or curved beam elements. A significantly greater mass and stiffness of the blocks in comparison to the masses and stiffnesses of the leaf springs ensure that the first two natural frequencies, as well as their corresponding vibration modes, for the most part agree with ones that would be calculated assuming that the springs do not

possess inertia and that the blocks were rigid. However, since the parameters of this system are distributed, additional natural modes appear which cannot be considered using the lumped parameter model at frequencies higher than its fourth dominant natural frequency.

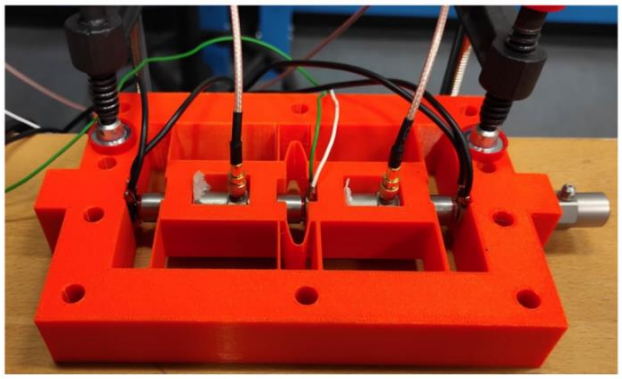

**Figure 4.** The photograph of the experimental setup

A convenient technology for the fabrication of such an experimental setup is 3D printing, as it enables a fast transition from a computer-generated model to a physical prototype using a CAD/CAM approach. A fused deposition modelling printer was used and PETG (Polyethylene Terephthalate Glycol modified) filament was used as the material. After the printing was complete, the mechanical part of the prototype was equipped with sensors and actuators.

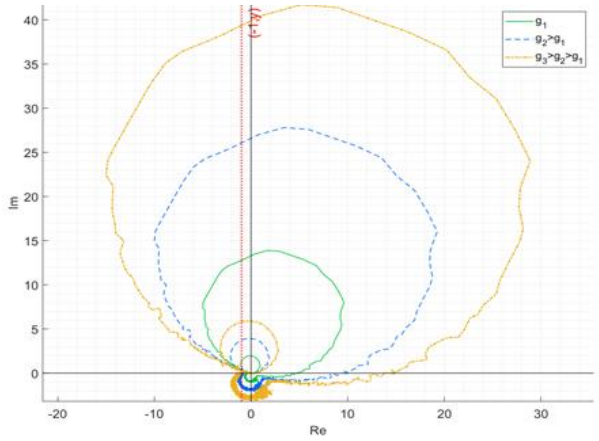


**Figure 5.** The Nyquist plot of the sensor-actuator open-loop FRF obtained experimentally.

It can be seen that the shape of the locus is quite similar to that obtained theoretically so that the maximum stable feedback gain is limited.

**Figure 6** shows the transfer mobility of the active system with increasing feedback gains obtained experimentally. The lowest antiresonance frequency is about 90 Hz and it corresponds to the inertance of about 30 grams. This is about five times the total mass of the voice coil actuator used to apply the control force (5.7 grams).

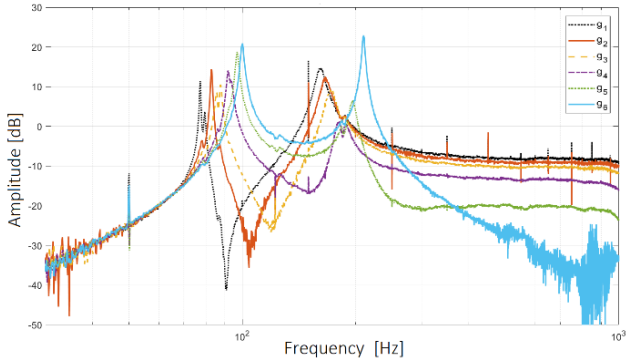


**Figure 6.** The transfer mobility of the active system with increasing feedback gains obtained experimentally.

By comparing **Figure 6** and **Figure 3**, the stability limit for theoretical case was associated with the antiresonance of around 220Hz which, while the one obtained with the experimental rig is close to 90Hz. That

indicates that the theoretical closed-loop system has smaller margin of stability then the experimental counterpart. This is associated with the fact that an additional simple first order Butterworth low-pass filter with a 1000Hz cut-off frequency is integrated within the feedback loop of the experimental setup, which considerably rotates the sensor-actuator open-loop FRF function clockwise, and significantly damps the transducer resonances. The effect of the filter is show in **Figure 7**, where the Nyquist plot of the sensor-actuator open-loop FRF with and without the low-pass filter is shown. The similarity with the contour observed in Fig. 5 is evident.

## 4. CONCLUSIONS

Inerter element is realised by means of feeding back the subtracted outputs of collocated inertial accelerometers to the voice coil actuator between the base and the sensitive equipment. Although the control approach is physically well-founded, its application is not straightforward. This is because although the relative acceleration sensor is collocated to the reactive force actuator, the two transducers are not dual i.e., they are not complementary in terms of mechanical power. As a result, the inherent frequency response of the sensor-actuator transducers inhibits the stability of the feedback loop. This requires the use of two low-pass filters. One is realised by using the voltage command to the voice coil actuator characterised by a resistance-inductance electrical cut-off frequency. Usable inertances can be realised which generate the desired antiresonance effect. Additionally, the antiresonance frequency can be easily tuned by varying the feedback gain. The maximum inertance is about 30 grams which is more than the weight of the actuator used.

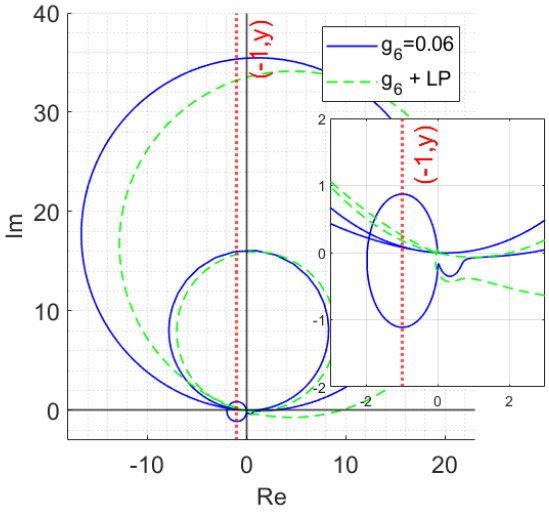


**Figure 7.** The Nyquist plot of the sensor-actuator open-loop FRF with (green dashed line) and without (blue solid line) 1000Hz low-pass filter.

## 5. ACKNOWLEDGMENTS

The Croatian Science Foundation HRZZ-IP-2019-04-5402 (DARS) support is gratefully acknowledged.

## 6. REFERENCES

[1] J.C. Schönfeld, Analogy of hydraulic, mechanical, acoustic and electric systems, Applied Scientific Research. 3 (1954) 417–450. https://doi.org/10.1007/BF02123920.

[2] M.C. Smith, Synthesis of mechanical networks: the inerter, IEEE Trans Automat Contr. 47 (2002) 1648–1662. https://doi.org/10.1109/TAC.2002.803532.

[3] J.M. Renno, B.R. Mace, Vibration modelling of helical springs with non-uniform ends, J Sound Vib. 331 (2012) 2809–2823. https://doi.org/10.1016/j.jsv.2012.01.036.

[4] M.C. Smith, F.-C. Wang, Performance Benefits in Passive Vehicle Suspensions Employing Inerters, Vehicle System Dynamics. 42 (2004) 235–257. https://doi.org/10.1080/00423110412331289871.

[5] R. Faraj, Ł. Jankowski, C. Graczykowski, J. Holnicki-Szulc, Can the inerter be a successful shock-absorber? The case of a ball-screw inerter with a variable thread lead, J Franklin Inst. (2019). https://doi.org/10.1016/j.jfranklin.2019.04.012.

[6] D. De Domenico, P. Deastra, G. Ricciardi, N.D. Sims, D.J. Wagg, Novel fluid inerter based tuned mass dampers for optimised structural control of base-isolated buildings, J Franklin Inst. (2018). https://doi.org/10.1016/j.jfranklin.2018.11.012.

[7] M.J. Brennan, J. Garcia-Bonito, S.J. Elliott, A. David, R.J. Pinnington, Experimental

investigation of different actuator technologies for active vibration control, Smart Mater Struct. 8 (1999) 145–153. https://doi.org/10.1088/0964-1726/8/1/016.

[8] A. Gonzalez-Buelga, L.R. Clare, S.A. Neild, J.Z. Jiang, D.J. Inman, An electromagnetic inerter-based vibration suppression device, Smart Mater Struct. 24 (2015) 055015. https://doi.org/10.1088/0964-1726/24/5/055015.

[9] J. Høgsberg, M.L. Brodersen, S. Krenk, Resonant passive-active vibration absorber with integrated force feedback control, Smart Mater Struct. 25 (2016) 047001. https://doi.org/10.1088/0964-1726/25/4/047001.

[10] G. Zhao, G. Raze, A. Paknejad, A. Deraemaeker, G. Kerschen, C. Collette, Active tuned inerter-damper for smart structures and its $\mathscr{H}\infty$ optimisation, Mech Syst Signal Process. 129 (2019) 470–478. https://doi.org/10.1016/J.YMSSP.2019.04.044.

[11] N. Alujević, D. Čakmak, H. Wolf, M. Jokić, Passive and active vibration isolation systems using inerter, J Sound Vib. 418 (2018) 163–183. https://doi.org/10.1016/J.JSV.2017.12.031.

[12] S.S. Rao, Mechanical vibrations, Prentice Hall, 2011.

[13] A. Preumont, Vibration Control of Active Structures, Springer International Publishing, Cham, 2018. https://doi.org/10.1007/978-3-319-72296-2.

[14] M.J. Balas, Direct Velocity Feedback Control of Large Space Structures, Journal of Guidance, Control, and Dynamics. 2 (1979) 252–253. https://doi.org/10.2514/3.55869.

[15] N. Alujević, I. Tomac, P. Gardonio, Tuneable vibration absorber using acceleration and displacement feedback, J Sound Vib. 331 (2012) 2713–2728. https://doi.org/10.1016/j.jsv.2012.01.012.

[16] Non-Comm DC Voice Coil Linear Actuator - NCC01-04-001-1X, (n.d.). https://www.h2wtech.com/product/voice-coil-actuators/NCC01-04-001-1X.